ELSEVIER

Respiration Physiology 128 (2001) 277–297

RESPIRATION PHYSIOLOGY

www.elsevier.com/locate/resphysiol

Bioenergetics at low oxygen: dependence of respiration and phosphorylation on oxygen and adenosine diphosphate supply

Erich Gnaiger *

D. Swarovski Research Laboratory, Department of Transplant Surgery, University Hospital Innsbruck, Anichstrasse 35, 6020 Innsbruck, Austria

Accepted 24 July 2001

Abstract

Oxygen limitation is generally considered as impairment of mitochondrial respiration under hypoxia and ischemia. Low intracellular oxygen levels under normoxia, however, imply mild oxygen limitation, provide protection from oxidative stress, and result from economical strategies for oxygen transport through the respiratory cascade to cytochrome *c* oxidase. Both perspectives relate to the critical oxygen pressure, which inhibits mitochondrial respiration. Based on methodological considerations of oxygen kinetics and a presentation of high-resolution respirometry, mitochondrial oxygen affinities ($1/P_{50}$) are reviewed with particular emphasis on the turnover effect under control of adenosine diphosphate ADP concentration, which increases the P_{50} in active states. ADP/O_2 flux ratios are high even under severe oxygen limitation, as demonstrated by calorespirometry. Oxygen limitation reduces the uncoupled respiration observed under control by ADP, as shown by relationships derived between ADP/O_2 flux ratios, respiratory control ratios, and ADP kinetics. Bioenergetics at low oxygen versus oxidative stress must be considered in the context of limitation of maximum aerobic activity, ischemia-reperfusion injury, mitochondrial signalling to apoptosis, and mitochondrial theories of ageing.

Keywords: Energy; oxidative phosphorylation; adenosine diphosphate kinetics; adenosine diphosphate/O_2 ratio; Hypoxia; mitochondrial O_2 kinetics; Mammals; rat; Membrane; permeability; Mitochondria; heart; liver

1. Introduction: two models of respiratory control

While numerous reviews highlight the biochemical and thermodynamic benefits of oxygen-dependent aerobic energy transformations in contrast to adenosine triphosphate ATP concentration production under anoxia (Hochachka and Somero, 1984; Gnaiger, 1993), an increasing body of literature is concerned with the various facets of oxygen toxicity and oxidative stress resulting from high oxygen levels. In the intracellular microenvironment, mitochondria are well separated from air-level oxygen pressure, and high rates of oxidative phosphorylation must be maintained near or at limiting oxygen levels in some tissues. On the

* Tel.: +43-512-504-4623; fax: +43-512-504-4625.
E-mail address: erich.gnaiger@uibk.ac.at (E. Gnaiger).

0034-5687/01/$ - see front matter
PII: S0034-5687(01)00307-3

other hand, mitochondria are routinely isolated and studied at unphysiologically high oxygen concentrations with limited additions of antioxidants, despite the fact that mitochondria in tissues are protected from oxidative stress by both low oxygen levels and complex defence systems against reactive oxygen species (ROS). Few studies, however, address the bioenergetic consequences of oxygen limitation on mitochondrial respiration and ATP production (Gnaiger et al., 2000b).

Mitochondrial and cellular respiration declines with a non-hyperbolic oxygen dependence by $\approx$ 10%, when oxygen pressure is decreased from 20 to 1 kPa (Gnaiger et al., 1995; Steinlechner-Maran et al., 1996). Another 10% oxygen limitation is incurred, when P_{O_2} is nine times the P_{50}, the oxygen pressure, where mitochondrial respiration is 50% reduced, according to the hyperbolic oxygen dependence found at $P_{O_2} < 1$ kPa. Mitochondrial P_{50} values are 5–20 times less than the half-saturation point of myoglobin, which then suggests that mitochondrial respiration operates at the edge of oxygen limitation under normoxic intracellular oxygen pressures (Gnaiger et al., 1998b).

Electron flux through the respiratory chain increases 10–20-fold during transitions between rest and work in active tissues, and corresponding changes in turnover rate of cytochrome *c* oxidase exert a direct influence on mitochondrial oxygen kinetics (Gnaiger et al., 1998b; Verkhovsky et al., 1996). P_{50} increases as a function of J_{max}, which is the oxygen flux at kinetic oxygen saturation under the control of adenosine diphosphate (ADP; Gnaiger et al., 1998a,b; St-Pierre et al., 2000b). At high oxygen levels, activity of isolated mitochondria is maximum at saturating ADP concentraion (state 3). Even when reducing ADP concentration towards zero (state 4), respiration of most mitochondrial preparations declines by a factor of < 10 (although respiratory control ratios > 20 are possible; Gnaiger et al., 2000a). State 4 oxygen consumption is maintained mainly to compensate for the proton leak through the inner mitochondrial membrane. The transition from high to low rates of respiration, therefore, is associated with a declining ATP yield per unit oxygen consumed, i.e. a diminished ADP/O_2 flux ratio under conditions of ADP limitation. In contrast, when mitochondrial respiration is oxygen limited by > 30 times below aerobic state 3 (five times below state 4), we found that the ADP/O_2 flux ratio was maintained high under hypoxia (Gnaiger et al., 2000b). The contrasting effects of ADP and oxygen limitation on phosphorylation efficiency are explained by their opposite relations to the mitochondrial membrane potential and uncoupled respiration, possibly including an increase of membrane permeability by high oxygen levels under oxidative stress. Thus, ADP and oxygen supply represent two experimental models for mitochondrial respiratory control of oxygen flux and ATP production. Their integration (Boveris et al., 1999; Chance et al., 1985; Gnaiger et al., 1998a,b; Jones, 1986) is the topic of the following presentation and may resolve questions left open, when excluding either one of these complementary perspectives.

2. Mitochondrial kinetics measured by high-resolution respirometry

Conventional respirometric techniques are not sensitive enough for studying oxygen kinetics of isolated mitochondria. To provide a routine approach to the study of oxygen kinetics, high-resolution respirometry was developed for accurate measurement with small amounts of tissue, cells and isolated mitochondria (0.04 mg mitochondrial protein, 10^6 endothelial cells, or 1.5 mg wet weight of muscle fibres in the 2 ml chamber). Measurement of mitochondrial P_{50} as low as 0.01 kPa (0.1 μM), at temperatures of 37 °C (Steinlechner-Maran et al., 1996) to 3 °C (St-Pierre et al., 2000b), rests on several tightly integrated features, particularly (a) instrumental design to achieve minimum oxygen diffusion into a homogenously stirred closed chamber (Fig. 1), (b) polarographic oxygen sensors (POS) and electronics providing sufficient stability and resolution of dissolved oxygen in a dynamic range of 10^4 between ≈ 200 μM O_2 at air saturation and 0.01% air saturation ($C_{O_2} = 0.02$ μM O_2; $P_{O_2} = 0.002$ kPa; Fig. 2), (c) high time resolution of the signal (Fig. 3), (d) software-supported mathematical signal correc-

tion based on standardized instrumental calibrations (Figs. 3 and 4), (e) resolution of non-linear changes of rate based on the time derivative of oxygen concentration (Figs. 4 and 5A and B), and (f) critical experimental design with adjusted mitochondrial or cellular concentrations, to match volume-specific respiratory activity with the limit of detection of oxygen flux and, on the other hand, with the limit of time resolution in aerobic–anaerobic transitions (Fig. 6, inset). In addition, a kinetically appropriate P_{O_2} range must be specified for non-linear curve fitting (Fig. 6; Gnaiger et al., 1995, 1998a).

2.1. The oxygraph for high-resolution respirometry

The OROBOROS *Oxygraph* (Oroboros Instruments, Innsbruck; and Paar, Graz, Austria) is a two-chamber titration-injection respirometer (Fig. 1). Homogenous oxygen levels for mitochondria in well-stirred suspension are obtained in the closed system. The chamber volume is 1.5–3 ml in most applications. The large inner diameter of the chambers (16 mm) provides space for additional electrodes, light guides and mechanical transducers. Each chamber is equipped with a POS with a large cathode (2-mm diameter). Sensitivity and signal-to-noise ratio increase and signal drift at zero oxygen decreases with increasing cathode area (Gnaiger and Forstner, 1983). By angular insertion of the oxygen sensor (Fig. 1), dead space is minimised and the cathode is placed into optimum position for stirring, contrary to the customary central insertion, where the cathode is exposed to minimum water current (Haller et al., 1994).

Artefacts due to oxygen diffusion into the chamber are minimised by using appropriate materials (Fig. 1). Avoiding Perspex chambers is essential owing to problems of back-diffusion of oxygen and lipid-soluble inhibitors such as rotenone. Teflon (polytetrafluoroethylene, PTFE) is an effective O_2 buffer with 10-fold higher oxygen solubility (106.0 μM kPa^{-1}) compared to

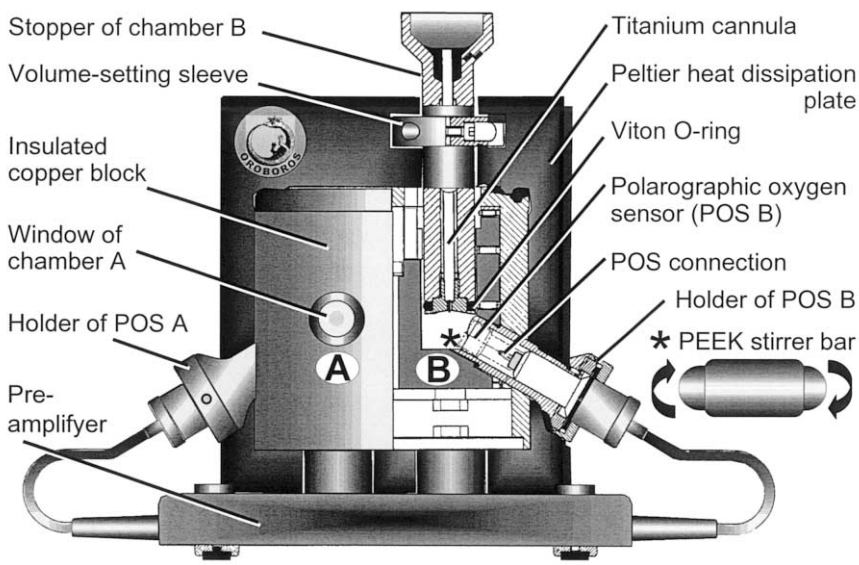

Fig. 1. The OROBOROS® *Oxygraph*. (A) Window into chamber A; (B) glass chamber B. Two chambers are housed in a temperature-regulated, *insulated copper block*. Peltier thermopiles are in thermal contact between copper block and *Peltier heat dissipation plate*. *Stopper of chamber B* (not shown for chamber A) with adjustable *sleeve* for setting the chamber volume, *titanium cannula* and conical titanium plate at the bottom, and *Viton O-ring* fitting against the cylindrical glass chamber. *POS* with butyl india rubber sleeve for sealing the POS against the glass chamber. Magnets generate a rotating electromagnetic field for driving the *PEEK stirrer bar* (polyetheretherketone; asterisk indicates position in chamber). *Pre-amplifiers* for the POS signal are housed in the base of the measuring unit.

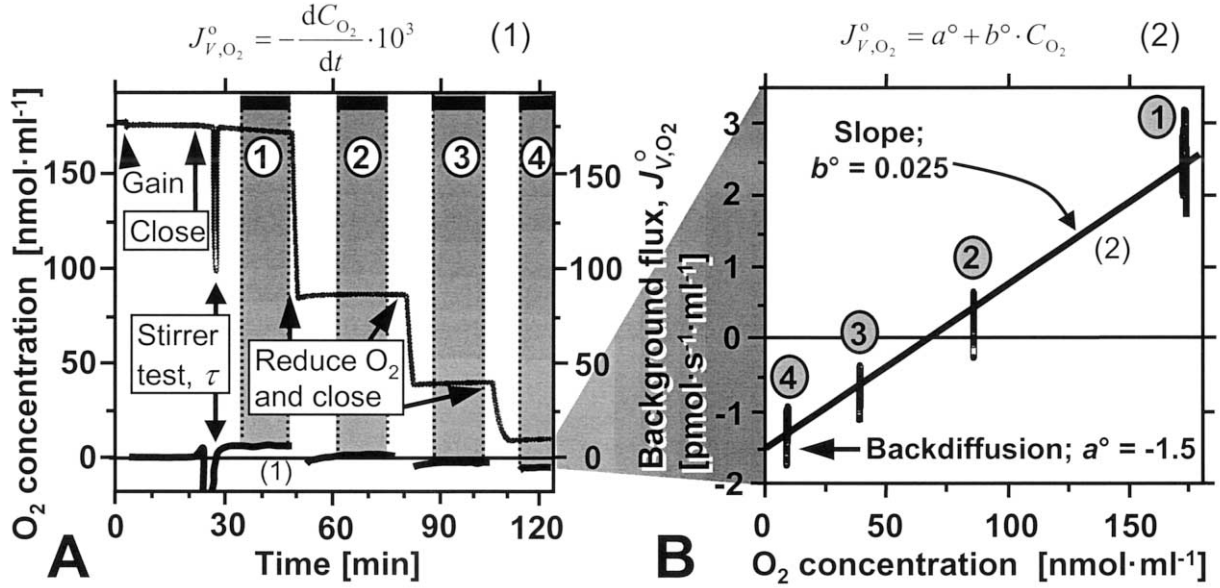

Fig. 2. Standard instrumental *Oxygraph* test using incubation medium without sample for air calibration, calibration of the time constant and of background oxygen flux. (A) *Upper trace*, oxygen concentration, C_{O_2} (μM = nmol ml^{-1}), and *lower trace*, volume-specific background oxygen flux, J^{o}_{V,O_2} (pmol sec^{-1} ml^{-1}; Eq. 1), recorded over time at sampling intervals of 1 sec. *Gain:* electronic gain setting, after equilibration between air space at partial insertion of the stopper (Fig. 1) and stirred incubation medium (2.2 ml culture medium RPMI, 37 °C, at digitally recorded barometric pressure of 95.5 kPa, oxygen solubility 9.4 nmol O_2 ml^{-1} kPa^{-1}). *Close:* the stopper is fully inserted, extruding air from chamber and titanium capillary of the stopper (185 μl), rendering a volume of 2.0 ml in the closed chamber (excluding volume of stirrer and capillary). *Stirrer test*, τ*:* rotation of both stirrers is switched off shortly and on, to calibrate the response time (Fig. 3A). *Reduce O_2 and close:* after partial opening of the stopper, argon is purged into the gas phase and the signal declines. At the desired oxygen level, the chamber is closed for recording instrumental background (marked Sections 1–4; excluding periods of stabilisation). (B) Background oxygen flux of Sections 1–4 plotted as a function of corresponding oxygen concentration. After zooming into the narrow range of flux, individual data points appear as vertical scatter bars. The linear regression is shown with intercept, a° (back-diffusion at zero oxygen concentration), and slope, b° (Eq. 2). These parameters yield a control of system performance and are used for instrumental background correction (Eq. 4).

incubation medium with lower solubility than water (12.6 μM kPa^{-1}; Gnaiger and Forstner, 1983; see also Hinkle et al. (1991)). For a 1.5 ml glass chamber, Lemasters (1984) reports a rate of back-diffusion of −9 pmol O_2 sec^{-1} ml^{-1} at 30% air saturation, compared to −1.5 to −3 pmol O_2 sec^{-1} ml^{-1} at zero oxygen in the OROBOROS *Oxygraph* with PEEK stirrers (Fig. 2B). This residual oxygen diffusion is probably mainly due to oxygen leakage from the electrolyte reservoir of the sensor into the sample medium. After some hours of equilibration at minimum oxygen levels, oxygen stores for back-diffusion are depleted and diffusion is zero over days recorded in the OROBOROS *Oxygraph*. Initial oxygen diffusion increases, however, by a factor of 10–30, when choosing a Teflon stirrer or wrong materials for sealings.

Temperature is regulated electronically at ± 0.05 °C by a built-in Peltier thermostat in the range 2–50 °C (at room temperature), yielding superior temperature stability compared with a conventional water jacket. The microprocessor controls independently the variable speed of two built-in electromagnetic stirrers. Optimum signal stability depends on the stirring rate, typically between 5 and 10 rotations per second (300–600 rpm). A slow-start function prevents decoupling of the stirrer magnet. An A/D converter transmits the signal of each chamber independently through an RS232 port at 1 sec intervals (minimum is 200 msec), after time averaging 30 readings. The digi-

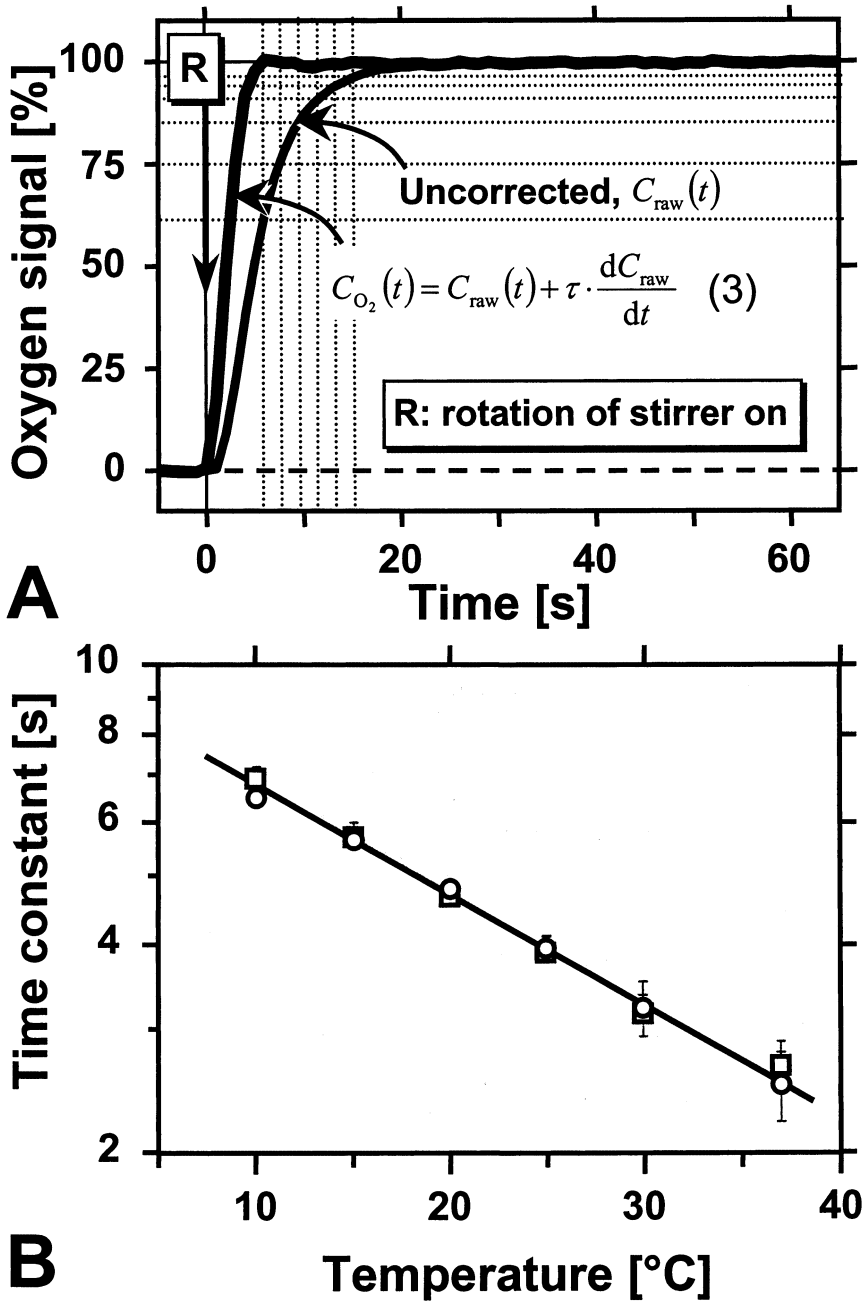

Fig. 3. Time response of the POS with a 25 μm FEP membrane (fluorinated ethylene–propylene). (A) Calibration of the exponential time constant by a stirrer test (Fig. 2). The oxygen signal is expressed in % of the total step change achieved by switching the stirrer on (arrow R) after local oxygen depletion at the membrane. A constant rotation speed of the stirrer is reached within a few seconds (first dotted line). An exponential fit of the *uncorrected* signal over the following period yields the time constant, τ (3 sec; 37 °C), which then is used for deconvolution of the signal (*corrected* concentration, $C_{O_2}(t)$; Eq. 3). (B) Effect of temperature on the time constant, τ, of two sensors, determined by titrations of 200–250 μl anoxic medium into chamber volumes of 2 ml at a stirring speed of 300 rpm. Each value represents the mean ± S.D. of 5–6 measurements (after Reck et al. (1997)).

tal limit of resolution is < 0.001 kPa ($< 0.005\%$ air saturation). Signal noise at P_{O_2} of 20 kPa is typically ± 0.005 kPa (0.03%) and is reduced with decreasing oxygen to ± 0.003 kPa, which is of particular importance for studies of oxygen kinetics (Gnaiger et al., 1995; Steinlechner-Maran et al., 1996). Noise is reduced further by smoothing, taking care not to compromise time resolution by inappropriate smoothing functions. These specifications (S.D. of 100 data points recorded at 1 sec intervals, without smoothing) set the limit of detection of volume-specific oxygen flux at 0.5 pmol sec^{-1} ml^{-1} at any oxygen level in the closed system (Fig. 2).

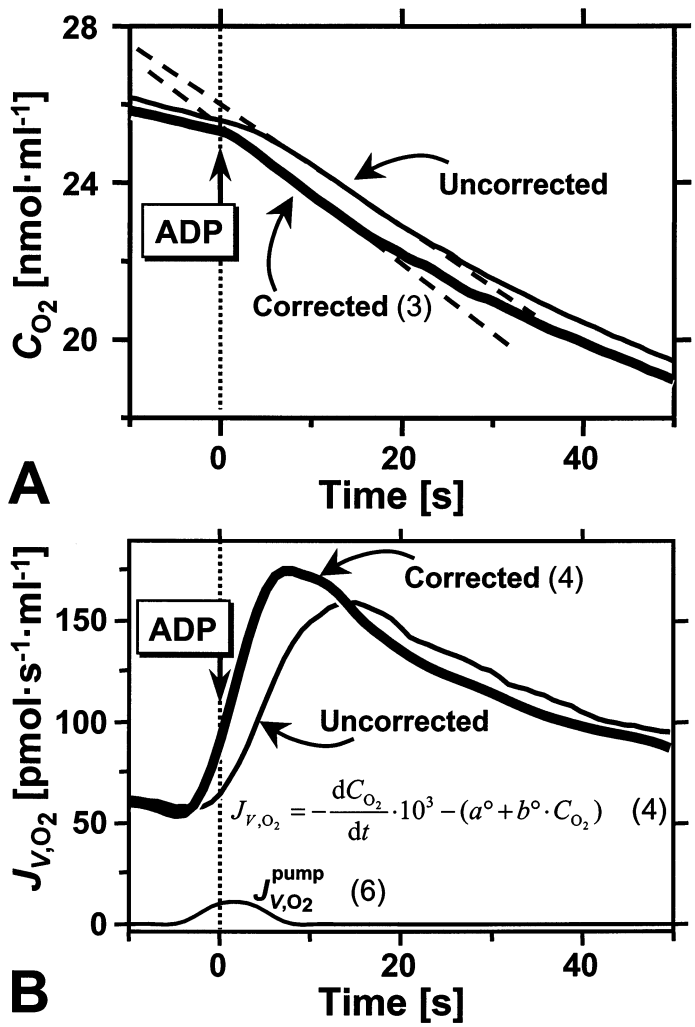

Fig. 4. Effect of time correction on oxygen concentration, C_{O_2} (A), and oxygen flux, J_{V,O_2} (B), following a titration of ADP (vertical arrows, initial concentration 15.5 μM) to isolated rat liver mitochondria (0.21 mg protein ml^{-1}). Heavy and thin lines are the time-corrected and uncorrected traces, respectively (exponential time constant of 5 sec; 25 °C). At low activation by ADP, the sharp peak of stimulated oxygen flux (2.9-fold above state 4 respiration) is underestimated in the uncorrected trace. Correction for the time response (Eq. 3) is important in initial rate kinetics, and maximum slopes (dashed lines, A) are difficult to determine in comparison to the peak of the time derivative (flux B; Eq. 4). The bottom line, $J_{V,O_2}{}^{pump}$, indicates the correction for the titration of 8.5 μl anoxic ADP solution (Eq. 6).

2.2. Calibrations and corrections for response time and instrumental background

Simultaneous on-line recording of oxygen concentration and oxygen flux (Eq. 1), and digital data analysis are a prerequisite for high-resolution respirometry and oxygen kinetics, supported by *DatLab* software (Oroboros Instruments) with specific signal corrections. A routine instrumental test is illustrated in Fig. 2, including calibration of the oxygen signal and time constant at air saturation and calibration of instrumental background oxygen flux. POS yield an electrical current proportional to the partial pressure of oxygen in the medium by consuming oxygen at 2.591 pmol O_2 sec^{-1} μA^{-1} in the cathode half reaction (Gnaiger and Forstner, 1983),

$$O_2 + 2H_2O + 4e^- \rightarrow 4OH^-$$

This explains background oxygen flux at air saturation of 2–3 pmol O_2 sec^{-1} ml^{-1} in a 2-ml chamber at 30–37 °C, and a linear decline of oxygen consumption towards zero oxygen (Fig. 2B). On the other hand, the rate of oxygen diffusion into the chamber depends linearly on the oxygen pressure difference between the oxygen source and the medium, being largest in the hypoxic region and decreasing linearly with increasing oxygen pressure. At zero oxygen, back-diffusion is typically -2 pmol O_2 sec^{-1} ml^{-1}. Combined with the oxygen consumption of the sensor, this results in linear slopes of $0.02–0.03 \times 10^{-3}$ sec^{-1}, when plotting background flux, J°_{V,O_2} (pmol sec^{-1} ml^{-1}), as a function of oxygen concentration, C_{O_2} (nmol ml^{-1}; Fig. 2B; Eq. 2). This oxygen dependence of instrumental background flux is applied for continuous correction of experimental oxygen flux over the entire oxygen range. At experimental oxygen flux of 100 pmol sec^{-1} ml^{-1}, instrumental background amounts to $< 3\%$. Because background effects increase with declining biological activity, corresponding corrections set a standard in high-resolution respirometry. Sensitivity is ± 1 pmol O_2 sec^{-1} ml^{-1} after background correction.

The signal of POS responds exponentially to rapid changes of oxygen pressure in the medium, which may be induced by pulse-titration of anoxic into air-saturated medium or by turning the stirrer off and on (Fig. 2A). Both methods yield identical results, which indicates that mixing is complete within a few seconds. The response is fitted to an exponential function to obtain the time constant, τ (Fig. 3A), which is calibrated routinely and improved occasionally by sensor service. The effect of signal deconvolution (Fig. 3A; Eq. 3) must be considered in all transient-state kinetic studies, as illustrated in pulse titrations with limiting ADP concentration, where an uncorrected signal would underestimate the initial rate (Fig. 4). In oxygen kinetics, underestimating or ignoring the response time results in an erroneous increase of P_{50}, particularly pronounced with increasing volume-specific oxygen flux. τ is typically 3–4 sec at 25–37 °C, and depends on experimental temperature as expected for a diffusion-controlled process (Fig. 3B). An increase in viscosity by addition of 10% dextran to the medium does not significantly affect the time constant. In addition, τ is virtually constant at strirrer speeds between 100 and 700 rpm in anoxic injection experiments, thus excluding a significant contribution of the mixing process to the response time.

2.3. Steady-state injection respirometry

Combination of the *Oxygraph* with an electronically controlled titration-injection micropump allows operation at quasi steady-states, offering a new flexibility in experimental design by combining the advantages of closed and open systems approaches. ADP-injection respirometry was developed for the determination of ADP/O_2 flux ratios in relation to ADP kinetics of isolated mitochondria (Fig. 5A and B). This is compared to oxygen-injection respirometry (Fig. 5C) and oxygen-injection calorespirometry (Fig. 5D). In all cases, mitochondrial respiration is stimulated to a constant, sub-maximal level by continuous injection of a substrate (ADP or oxygen), which is consumed by internal metabolism at a rate exactly matching the rate of injection at steady-state (Eq. 8). Importantly, injection flux must be chosen below the limit of mitochondrial capacity to prevent substrate concentrations in the medium from

$$J_{V,O_2} = -\frac{dC_{O_2}}{dt}10^3 - \left(J^{o}_{V,O_2} + J^{pump}_{V,O_2}\right) \quad (5)$$

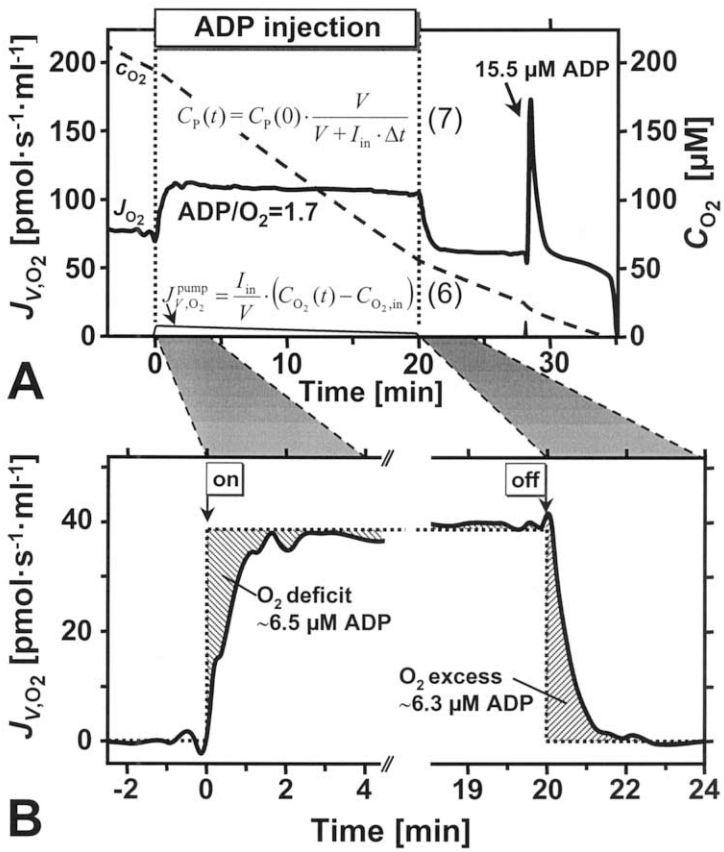

Fig. 5. ADP-injection respirometry and oxygen-injection calorespirometry with rat liver mitochondria (25 °C, succinate and rotenone; Gnaiger et al., 2000b). (A) Activation of resting respiration (state 4, 2 mM ATP) by steady-state ADP-injection (20 min), ADP titration (Fig. 4), followed by aerobic–anaerobic transition for analysis of oxygen kinetics (Fig. 6). During injection, respiratory flux, J_{V,O_2} (Eq. 5), is obtained by adding to Eq. (4) a second correction term for injected and ejected oxygen flux, $J_{V,O_2}{}^{pump}$ (Eq. 6). This increases with the ratio of injection flow to chamber volume, I_{in}/V, and is most accurately calculated, when using an anoxic ADP-injection solution ($C_{O_2,in} = 0$). The oxygen concentration in the ejected medium is equal to $C_{O_2}(t)$ in the mixed medium in the chamber. Initial mitochondrial protein concentration, $C_P(0)$, was 0.21 mg ml^{-1}. Assuming complete mixing in the stirred chamber, the final protein concentration, $C_P(t)$, is calculated with Eq. (7). The wash out effect was $< 4\%$ at I_{in} of 0.10–0.20 µl sec^{-1} over periods, Δt, of 360–1200 sec. At steady-state, influx of substrate i (ADP or oxygen) into the chamber sets the mitochondrial metabolic flux, $J_{V,i}$ (pmol sec^{-1} ml^{-1}; Eq. 8). The substrate concentration in the injection solution is much higher than the steady state concentration in the chamber, $C_{i,in} \gg C_i$. With $I_{in} = 0.10$ µl sec^{-1}, $C_{ADP,in} = 4752$ µM and $V = 2.6$ ml, mitochondrial ADP flux, $J_{V,ADP}$, was set at 183 pmol O_2 sec^{-1} ml^{-1} (Eq. 8). $J_{V,ADP}$ divided by steady-state J_{V,O_2} yields directly the ADP/O_2 flux ratio under conditions of ADP-limited respiration. (B) Transition periods of ADP-injection and calculation of steady-state ADP concentration for ADP kinetics (Fig. 8A). Net oxygen flux above state 4 is shown for strictly methodological reasons. Steady-state is confirmed by identity of areas for *O_2 deficit* and *O_2 excess* (*hatched*), obtained by integration of oxygen

$$J_{V,i} = \frac{I_{\text{in}} \cdot (C_{i,\text{in}} - C_i)}{V} \qquad (8)$$

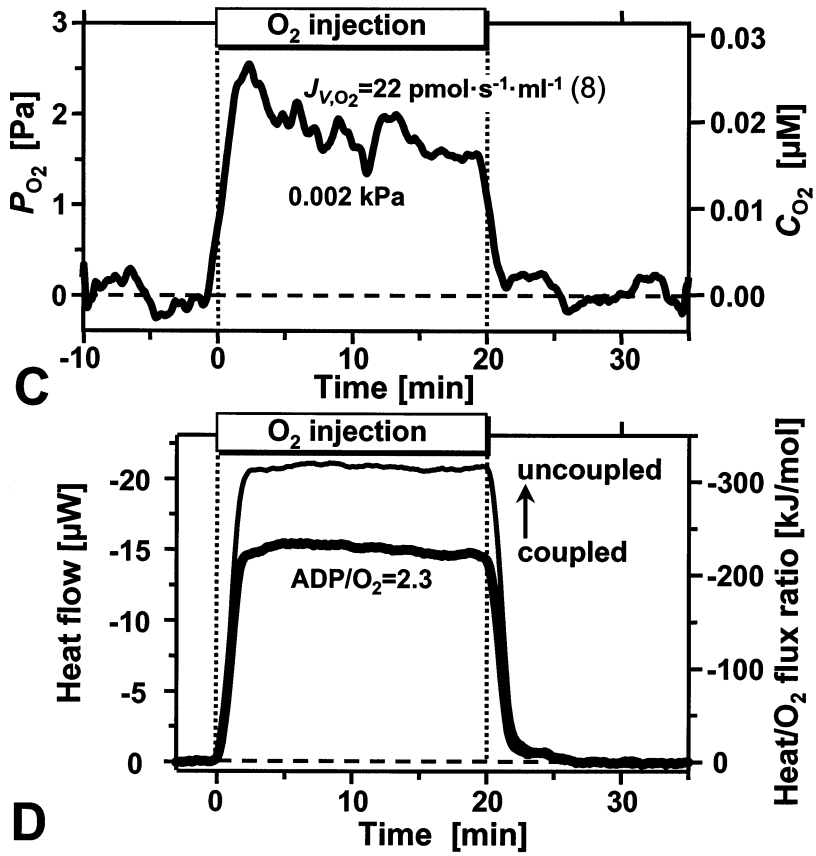

consumption relative to the ideal square wave (*dotted lines*). The O_2 deficit is proportional to initial ADP accumulation in the medium after switching ADP-injection on. The O_2 excess reflects the phosphorylation of accumulated ADP, comparable to a pulse titration of ADP (Fig. 5A). ADP/O_2 ratios (Fig. 5A) are used to convert the O_2 deficit and O_2 excess to the steady-state ADP concentration maintained during ADP-injection. (C) Steady-state O_2 injection, monitoring the hypoxic oxygen regime in the respirometer, preceded and followed by anoxic conditions used for internal zero calibration and correction for non-linear zero drift. P_{O_2} at steady state is regulated by the oxygen affinity of mitochondrial respiration, and was 0.0019 kPa $\pm$ 0.0002 S.D. (0.014 mmHg or 0.02 µM O_2; $N = 3$). With $I_{in} = 0.3$ µl sec^{-1}, $C_{O_2,in} = 220$ µM, V = 3 ml and $C_P = 0.43$ mg ml^{-1}, oxygen-limited respiration was 0.05 nmol sec^{-1} mg^{-1}, compared to J_{max} of 0.21 nmol sec^{-1} mg^{-1} ($\pm$0.02 S.D.). (D) Oxygen-injection calorespirometry at limiting oxygen supply (0.05 nmol O_2 sec^{-1} mg^{-1} protein). In the first section of the experiment, respiration was coupled to oxidative phosphorylation, whereas the mitochondria were chemically uncoupled in the second section (superimposed). Because, oxygen flux was identical for both treatments, the measured heat flow (µW = µJ sec^{-1}; left ordinate) is directly proportional to the heat/O_2 flux ratio (right ordinate). The uncoupled heat/O_2 flux ratio averaged -320 kJ mol^{-1} ($\pm$14 SEM; $n = 8$) in direct agreement with the theoretical oxycaloric equivalent of -309 kJ mol^{-1} for oxidation of succinate to fumarate and malate. Less negative coupled heat/O_2 flux ratios are due to the enthalpy conserved in the phosphorylation of ADP–ATP (44 kJ mol^{-1} ATP), yielding an ADP/O_2 ratio of 2.3 ($\pm$0.4 SEM; $n = 4$). Heat flux was measured in a titration vessel of a 2277 Thermal Activity Monitor (Thermometric, Järfälla, Sweden). The signal was corrected for τ of 240–280 sec and non-linear baseline drift.

increasing continuously above saturating levels. A 500 μl glass syringe with tightly connected stainless steel capillary prevents oxygen diffusion into the anoxic ADP-injection solution (Fig. 5A). Injection flows can be regulated at intervals of 0.01 μl sec^{-1} over selected periods of time. Sequences of injections and fast pulse titrations are defined in set-up programs. The injection capillary is inserted into the chamber closely above the rotating stirrer rod long before the injection is switched on automatically, to obtain undisturbed transitions (Fig. 5B) and prevent interferences with the oxygen signal (Fig. 5C).

Continuous ADP-injection may be compared with application of ADP regenerating enzyme systems (hexokinase or creatine kinase) for stimulation of mitochondrial respiration (Jacobus et al., 1982; Stoner, 1987). Advantages of steady-state ADP-injection for measurement of the ratio of ADP flux to oxygen flux (ADP/O_2 flux ratio) are the options to (a) regulate ADP flux accurately, (b) observe the transition to state 4 after stopping the pump, (c) derive the ADP concentration without rapid termination of the reaction and subsequent chemical analyses, and (d) use physiologically relevant high ATP concentrations

$$\frac{J_{O_2}}{J_{max}} = \frac{P_{O_2}}{P_{50} + P_{O_2}} \qquad (9)$$

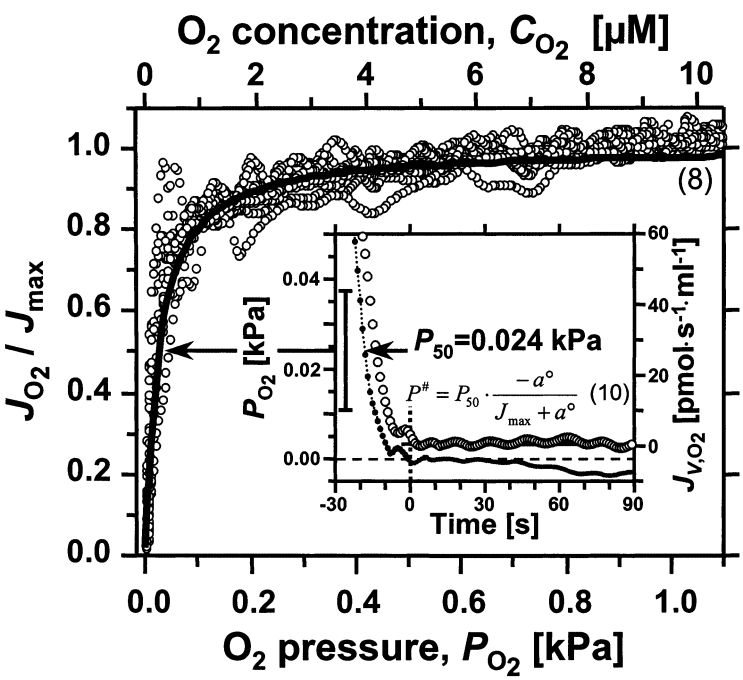

Fig. 6. Oxygen kinetics of isolated rat liver mitochondria (state 4; experimental conditions as in Fig. 5). Respiratory rate is normalised relative to oxygen flux at kinetic oxygen saturation, J_{max} (Eq. 9). *Full line* shows average hyperbolic fit (6 preparations; 1–3 replica each; vertical bar in inset shows mean $P_{50} = 0.024 \pm 0.013$ kPa S.D.). Individual data points are shown by symbols. Mitochondrial protein concentration ranged from 0.22 to 0.58 mg ml^{-1}, yielding $J_{V,max}$ of 50–130 pmol O_2 sec^{-1} ml^{-1} and 100–300 data points in the standardised oxygen range of 1.1–0.0 kPa (from Gnaiger et al. (2000b)). Inset: individual record, showing the oxygen range 2 P_{50} (after Méndez and Gnaiger (1994)). Time zero indicates completion of the aerobic–anaerobic transition, followed by the period of zero current drift of the signal (equivalent to 0.18 pmol sec^{-1} ml^{-1} in the example, compared to J_{max} of 98 pmol sec^{-1} ml^{-1}). Internal zero calibration is performed at this point, on the basis of iterative calculation of the oxygen pressure, $P^{\#}$ (Eq. 10), at which mitochondrial respiration compensates for back-diffusion of oxygen into the chamber, $J^{\#} = -a°$ (Eqs. 2–9; Gnaiger et al., 1995). $P^{\#}$ is 0.1×10^{-3} kPa in this example, i.e. far below the limit of detection of the oxygen sensor and in the same order of magnitude as the thermodynamic limit of the anoxic respiratory chain.

(Fig. 5B). With 2 mM ATP in the incubation medium, all added ADP is phosphorylated to ATP, because relative changes of ATP concentration are small and ATP/ADP ratios are effectively identical before and after ADP additions (Gnaiger et al., 2000b). Under these conditions, it is not necessary to consider corrections for an increase of ADP concentration after return to state 4 (Hinkle et al., 1991). It is important, however, to use mitochondrial preparations with minimum ATPase activity and hence minimum ATP-turnover in state 4. This is tested by stimulation of respiration in state 2 (no adenylates) to state 4 by addition of ATP or inhibition of state 4 respiration by oligomycin. Low ATPase activity in our rat liver mitochondrial preparations was reflected by respiratory control ratios (state 3/state 4) of 7–8 (Méndez and Gnaiger, 1994; Gnaiger et al., 2000b). ATP stimulation was significantly reduced by application of a new preservation medium, for storage of heart mitochondria on ice between isolation and respirometric incubation (Gnaiger et al., 2000a). Presumably, the complex mixture of anti-oxidants is mainly responsible to prevent activation of mitochondrial ATPases shortly after isolation.

Oxygen-injection respirometry (Fig. 5C) does not yield information on ADP fluxes under hypoxia. We developed, therefore, oxygen-injection calorespirometry to answer the question, whether mitochondrial ATP production is possible under severe oxygen limitation, when respiration is suppressed below maintenance levels (Gnaiger et al., 2000b). In this microcalorimetric approach, the thermodynamic efficiency of ATP production is measured directly in terms of enthalpy changes. When related to the controlled oxygen flux, ADP/O_2 flux ratios are obtained under conditions of hypoxia (Fig. 5D).

3. Mitochondrial respiratory control at low oxygen

3.1. Apparent oxygen affinity and catalytic efficiency of mitochondrial respiration

The oxygen dependence of mitochondrial respiration can be described by a hyperbolic function in the P_{O_2} range < 1.1 kPa (Fig. 6; Eq. 9). Analogous to the apparent K_m of an isolated enzyme, the P_{50} is the partial oxygen pressure at which flux is half maximal, and $1/P_{50}$ is the apparent affinity. Extremes of published P_{50} values for respiration of isolated muscle mitochondria in state 3 span a 30-fold range from 0.005 kPa (Cole et al., 1982) to 0.15 kPa (Costa et al., 1997). The very high affinity of mitochondrial respiration with correspondingly low $P_{50} < 0.01$ kPa was not confirmed by reference to intracellular myoglobin saturation as a signal for intracellular P_{O_2} (Wittenberg and Wittenberg, 1985; Kreutzer and Jue, 1995), phosphorescence quenching (Rumsey et al., 1990), nor by high-resolution respirometry (Gnaiger et al., 1995, 1998a,b, 2000b; Sharpe and Cooper, 1998; Steinlechner-Maran et al., 1996; St-Pierre et al., 2000b; Verkhovsky et al., 1996). Uncritical reference to the lowest reported P_{50} value yields a biased concept on the independence of mitochondrial respiration from intracellular oxygen pressure (Gayeski and Honig, 1991; Wittenberg and Wittenberg, 1989).

High volume-specific oxygen flux (at high mitochondrial protein concentrations) cause artefacts with entirely opposite effects on P_{50} measured by different instruments. In a respirometer with steady-state oxygen transfer from a gas phase to the aqueous phase, high oxygen flux is associated with large gradients between the oxygen source and mitochondria, particularly through the gas-aqueous phase boundary layer. Then the signal of the oxygen sensor at the bottom of the chamber is lower than average mitochondrial P_{O_2}, leading to underestimation of the P_{50} at a mitochondrial protein concentration of 10 mg ml^{-1} (Cole et al., 1982). Even when omitting a gas-aqueous boundary layer by direct oxygen-injection of air saturated solution into the stirred mitochondrial suspension, the P_{O_2} of 0.002 kPa measured at steady-state oxygen flux limited to 21% of J_{max} (Fig. 5C) was 50% lower than the P_{O_2} calculated from closed-chamber kinetics (Fig. 6). This discrepancy is expected, if respiration of a fraction of mitochondria is stimulated by high oxygen levels before mixing is complete and if the oxygen signal represents the P_{O_2} after mixing rather than a true volume-average. It is intuitively clear that the corresponding underestimation of P_{50} would be

accentuated at higher mitochondrial concentrations (>0.5 mg ml^{-1}), when a larger fraction of supplied oxygen is consumed before mixing is complete. In a closed system, on the other hand, an erroneously high P_{50} of 0.1 kPa results from increasing mitochondrial density to >0.2 mg ml^{-1} and hence volume-specific oxygen flux to >500 pmol sec^{-1} ml^{-1} (Gnaiger et al., 1998a). This may explain the high P_{50} reported for 0.2–0.5 mg ml^{-1} rat heart mitochondria in state 3 (Costa et al., 1997). Correct P_{50} values are measured in the passive state 4 at such high mitochondrial concentrations, but in state 3 the P_{50} of rat heart mitochondria is 0.035 kPa (± 0.016 S.D.), independent of mitochondrial protein concentration in the range of 0.02–0.12 mg ml^{-1} (Gnaiger et al., 1998a). This independence of volume-specific flux and aerobic–anaerobic transition time provides an important test for the validity of instrumental calibrations and corrections (Lassnig et al., 1998), including the essential internal zero oxygen calibration (Fig. 6; Eq. 10). Integration of the hyperbolic relation (Eq. 9) rather than differentiation (first term of Eq. (4)) has been suggested for closed-chamber respirometry (Froncisz et al., 1985), but it is more practical to apply instrumental corrections to the differentiated data (flux) and plot flux as a function of oxygen pressure (Fig. 6).

It is well established that uncoupling of oxidative phosphorylation causes the oxygen affinity of mitochondrial respiration to increase, particularly, when measured after inhibition to resting-level respiration (Rumsey et al., 1990; Steinlechner-Maran et al., 1996). Uncoupling is frequently used as a model for the active state of cells, with the explicit assumption that the low P_{50} of uncoupled mitochondria is due to the lower phosphorylation state ratio and thus representative for oxygen affinity in the active state 3 (Rumsey et al., 1990; Takahashi et al., 1999). If the P_{50} were actually decreased in the ADP-activated state at high flux (Wilson et al., 1979), the ADP control ratio would increase under hypoxia by a factor of up to $P_{50,4}/P_{50,3}$ (Eq. 11; Fig. 7B). In contrast, a kinetic model of cytochrome *c* oxidase predicts a proportional increase of P_{50} with enzyme turnover rate (Chance et al., 1985; Verkhovsky et al., 1996). In agreement with this model, we found an increase of P_{50} with J_{max} (Fig. 7A; Gnaiger et al., 1998a,b).

The increase of $P_{50,3}$ in the active state compared to $P_{50,4}$ in the resting state 4 is more pronounced in mitochondria from liver (0.057 kPa) than heart (0.035 kPa; Gnaiger et al., 1998b). In both cases, J_{max} accelerates more steeply with ADP activation than P_{50}. Hence, the apparent catalytic efficiency, J_{max}/P_{50}, increases while the apparent affinity, $1/P_{50}$, decreases with mitochondrial power output (Fig. 7A, arrow from dashed to dotted line). Whereas kinetic constraints prohibit the theoretically advantageous reduction of P_{50} at high activity and increased oxygen demand, the high catalytic efficiency in the active state is of direct functional importance for ATP production under hypoxia. On the other hand, a constant J_{max}/P_{50} ratio would imply that oxygen limitation causes a rapid decline of the ADP control ratio, $RCR_{3/4}$, the respiratory rate at state 3 relative to the rate at state 4 (Fig. 7B). Consequently, hypoxia would not only restrict respiratory rate, but energy limitation might be accentuated by the loss of coupling under low oxygen conditions. Contrary to the finding of Cole et al. (1982), uncoupling of oxidative phosphorylation has been reported to occur at low oxygen pressure (Kramer and Pearlstein, 1983), just as the ADP control ratio and ADP/O_2 flux ratio decline at low ADP concentrations (Fig. 8). Clarification of the ATP yield per unit oxygen consumed (ADP/O_2 flux ratio), therefore, is of fundamental importance for bioenergetic evaluation of respiration at intracellular low oxygen levels.

3.2. Effect of ADP and oxygen limitation on ADP/O_2 flux ratios

Inhibition of oxygen flux by ADP limitation (state 4) relative to ADP saturation (state 3) provides a test for well coupled heart or liver mitochondria, as expressed by the respiratory ADP control ratio. Measurement of ADP kinetics is difficult at low intracellular oxygen levels. Hence, an effectively hyperoxic P_{O_2} is used conventionally up to air saturation to study the dependence of mitochondrial respiration on ADP concentration in the presence of high phosphate and substrate concentrations (Fig. 5A). Well established over the past 50 years (Chance and Williams, 1955),

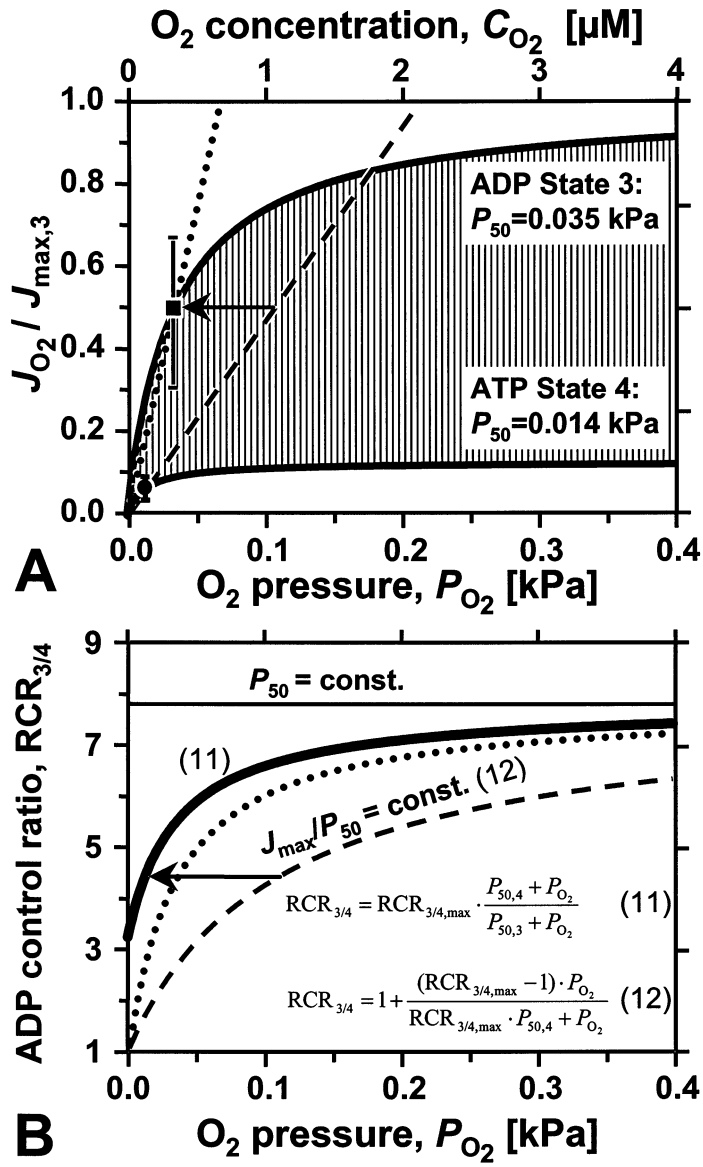

Fig. 7. Oxygen dependence of respiration in isolated rat heart mitochondria, and ADP control ratios as a function of oxygen pressure (30 °C, pyruvate and malate; Gnaiger et al., 1998a). (A) Oxygen kinetics in active state 3 (with 1 mM ADP and 1 mM ATP) and passive state 4 (with 1 mM ATP only). Flux is normalised to maximum oxygen flux calculated for state 3 respiration, $J_{max,3}$, of 4.6 nmol O_2 sec^{-1} mg^{-1} mitochondrial protein. Vertical lines indicate the range of activation by ADP at any P_{O_2}. Symbols show average P_{50} in state 4 and 3 (error bars are SD; $N = 9$ and 26, respectively). Dotted and dashed lines intersecting P_{50} yield slopes (0.5 J_{max}/P_{50}) proportional to the apparent catalytic efficiency, which increases with activation by ADP (arrow). (B) ADP control ratio ($RCR_{3/4}$, respiratory control ratio of oxygen flux at state 3 and 4), as a function of P_{O_2}, showing the decline of scope for activation under hypoxia (*heavy line*, Eq. 11). $RCR_{3/4,\,max} = J_{3,\,max}/J_{4,\,max}$ was 7.8; $RCR_{3/4} = 1$ indicates a zero scope for ADP activation. For the theoretical case of constant P_{50} in state 4 and 3, $RCR_{3/4}$ is constant and independent of P_{O_2} (*horizontal line*). For a theoretically constant catalytic efficiency (J_{max}/P_{50} = constant; Eq. 12), the $RCR_{3/4}$ declines to 1 at zero oxygen (*dashed line*, for J_{max}/P_{50} measured at state 4, $P_{50,3}$ would equal 0.109 kPa; *dotted line*, for J_{max}/P_{50} measured at state 3, $P_{50,4}$ would equal 0.0045 kPa).

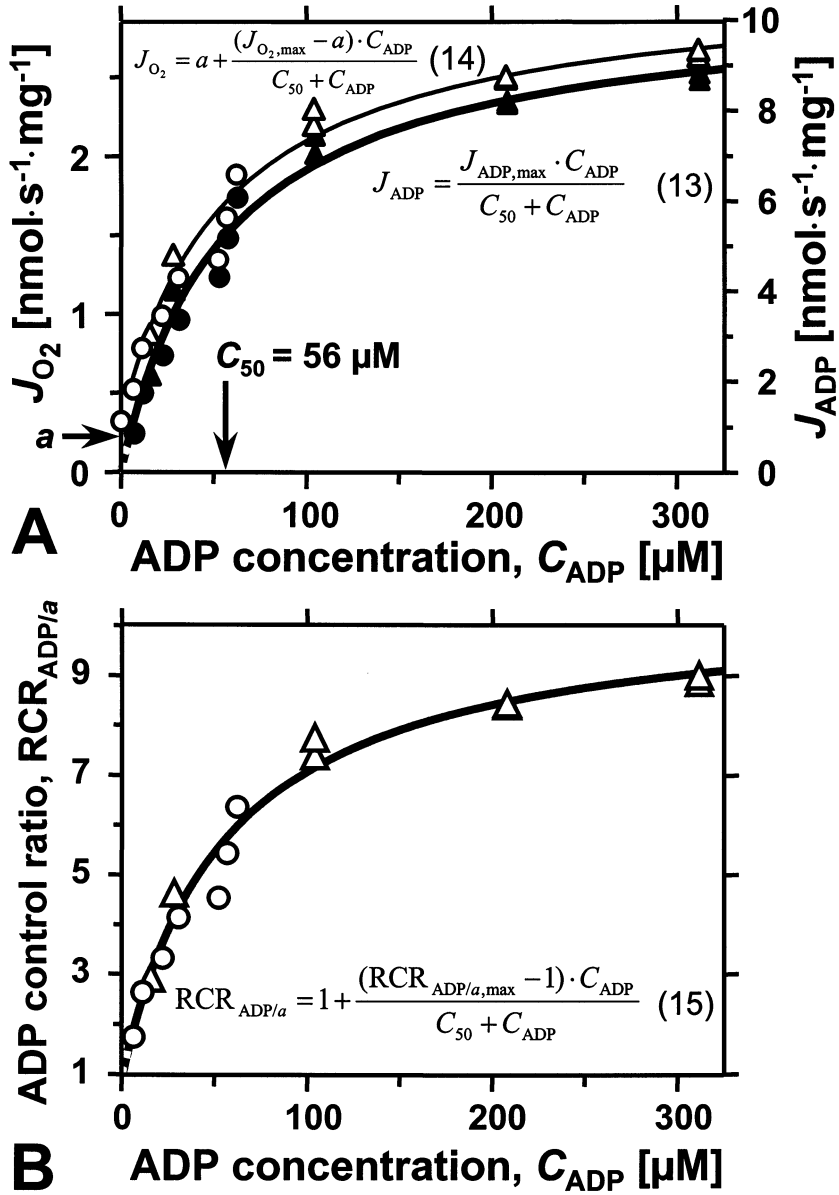

Fig. 8. ADP dependence of respiration at kinetic oxygen saturation of isolated rat liver mitochondria, corresponding ADP control ratios and ADP/O_2 flux ratios as a function of ADP concentration. Triangles are from ADP pulse titrations (Fig. 4), circles from ADP steady-state injections (Fig. 5A and B). (A) ADP kinetics of ADP flux, J_{ADP} (*closed symbols*; Eq. 13), and oxygen flux, J_{O_2} (*open symbols*; Eq. 14). Intercept a was significantly lower than state 4 ($a = 0.22 \pm 0.02$ SE; $n = 32$; 6 mitochondrial preparations; identical to the intercept in Eq. 18; Fig. 9A). (B) ADP control ratio ($RCR_{ADP/a} = J_{O_2}/a$; Eq. 15) as a function of ADP concentration, showing the decline in the scope for activation under ADP limitation. $RCR_{ADP/a,max} = J_{O_2,max}/a = 10.5$. Importantly, conventional respiratory ADP control ratios are lower ($RCR_{3/4} = 7.7$; state 3/state 4 flux ratio measured at 300 µM ADP). Owing to large effects of small changes in state 4 respiration compared to intercept a, the corresponding $RCR_{3/a}$ was 8.9 ($J_{O_2,3}/a$ at 300 µM ADP in the same experiment). Note these distinctions in comparison to Fig. 7. (C) ADP/O_2 flux ratio ($Y_{P/O_2} = J_{ADP}/J_{O_2}$; Eq. 16) as a function of ADP concentration, showing the decline of phosphorylation yield under ADP limitation. $Y_{P/O_2,\ max} = J_{ADP,\ max}/J_{O_2,max} = 3.4$. (D) ADP/$O_2$ flux ratio as a function of ADP control ratio, $RCR_{ADP/a}$. Inset: linearization by the inverse ADP control ratio, $RCR_{a/ADP}$ (Eq. 17). The intercept equals P/O_2 (compare Eq. (18)). 50% P/O_2 is reached at $RCR_{ADP/a} = 2$ or $RCR_{a/ADP} = 0.5$ (*vertical arrows*). (A–C) are from a single mitochondrial preparation, (D) includes data from 6 preparations.

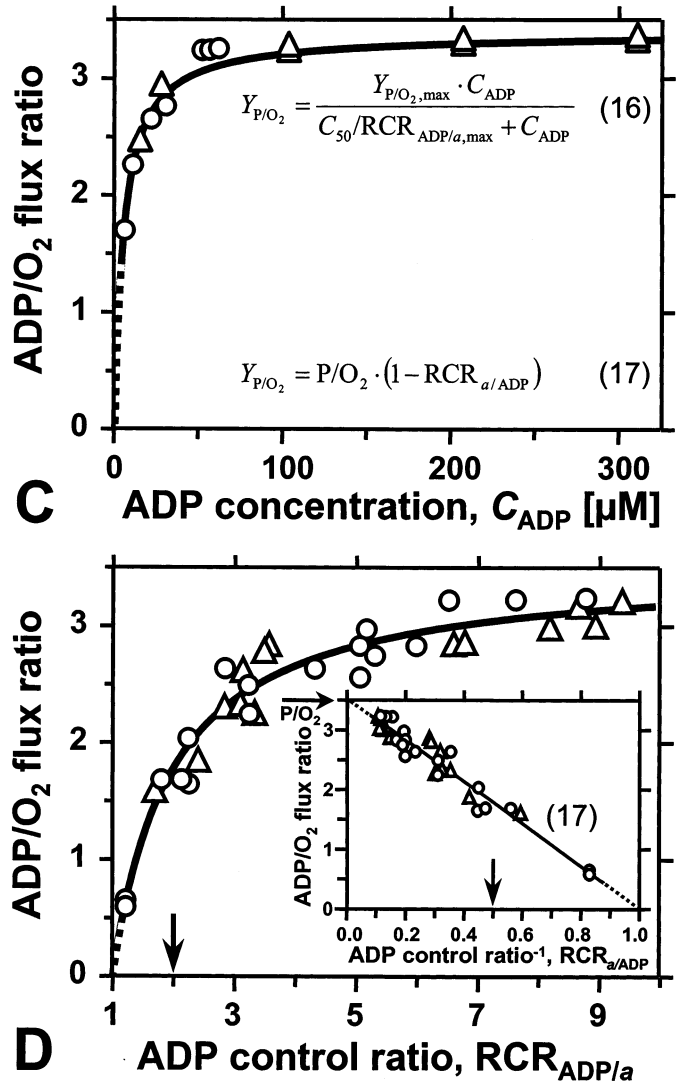

Fig. 8. (*Continued*)

oxygen flux above state 4 (strictly above a; see below) and ADP flux, i.e. the rate of phosphorylation of ADP–ATP, are hyperbolic functions of ADP concentration (Fig. 8A). The apparent $K_{m,ADP}$ or C_{50} (Eqs. 13 and 14) was 56 μM ADP, which is comparatively high owing to the physiologically realistic high ATP concentration (Jacobus et al., 1982). Considering the eminent importance ascribed in bioenergetics to the closely related respiratory control ratios and ADP/O_2 flux ratios, it is surprising that a rigorous quantitative derivation of their interdependence appears to be lacking. Based on (a) the hyperbolic dependence of ADP flux on ADP concentration (Fig. 8A), and (b) the linear increase of the rate of phosphorylation with respiratory rate (Fig. 9A), a set of equations can be derived to describe the hyperbolic dependence of ADP/O_2 flux ratios on ADP concentration, respiratory ADP control ratio and rate of respiration (Figs. 8 and 9).

In this context, the only directly linear relation is found between ADP flux and oxygen flux (Fig.

9A). Representation of oxygen flux on the X-axis is chosen merely for illustration (compare Gnaiger et al. (2000b)), whereas ADP flux is properly used as the independent variable for linear regression analysis (Eq. 18; J_{ADP} is strictly independent and under the control of the experi-

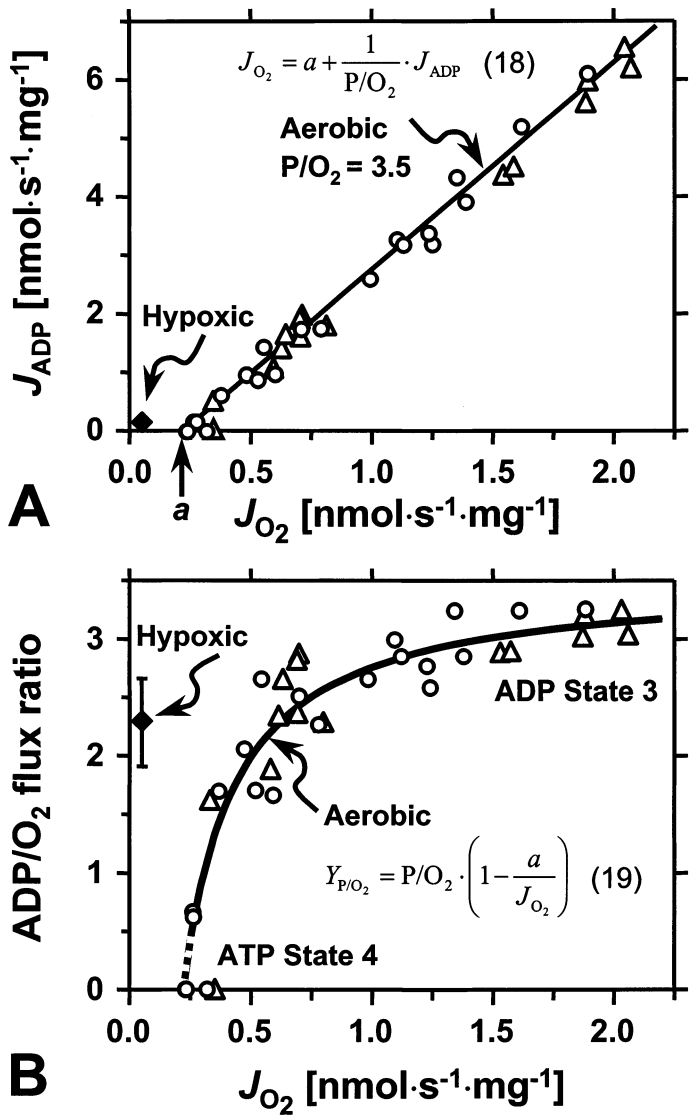

Fig. 9. ADP flux and ADP/O_2 flux ratio in relation to oxygen flux, J_{O_2}, in isolated rat liver mitochondria (Fig. 8). (A) Linear slope between ADP flux, J_{ADP}, and oxygen flux (Eq. 18). Full agreement was established between the steady-state fluxes obtained by ADP-injection respirometry (*circles*) and average fluxes in ADP-pulse respirometry (*triangles*). The latter were calculated by dividing the initial ADP concentration and the integrated oxygen concentration by the time interval of the oxygen peak (Gnaiger et al., 2000b). (B) ADP/O_2 flux ratio, Y_{P/O_2}, as a function of oxygen flux, J_{O_2}, under aerobic conditions compared to the hypoxic condition (SE bars). Aerobic ADP/O_2 ratios fall markedly as oxygen flux becomes progressively ADP limited under aerobic conditions (Eq. 19). In contrast, under severe oxygen limitation of respiration even below state 4 levels, ADP/O_2 ratios are maintained high (modified after Gnaiger et al., 2000b).

menter in steady-state ADP-injection; Fig. 5A). Calculation of intercept a is statistically most robust with linear Eq. (18), and is then used as a constant rather than parameter in Eq. (14). Importantly, measured state 4 respiration (in the presence of ATP) is marginally, but significantly higher than intercept a, when analysed separately for an individual mitochondrial preparation. Values of state 4 respiration, therefore, are not included in the regression analysis, to avoid the erroneous assumptions of zero ADP concentration at state 4 (Fig. 8A) and linearity in the narrow region between state 4 and oxygen flux at minimal ADP activation (Fig. 9A). An ADP respiratory control ratio, $RCR_{ADP/a}$, is defined for oxygen flux as a function of ADP concentration, divided by a. Of course, the dependence on ADP concentration is identical for ADP flux and $RCR_{ADP/a}$ (Fig. 8B; Eq. 15). It is interesting to note, however, that the ADP/O_2 flux ratio increases much more steeply with ADP concentration, becoming 'half-saturated' at $C_{50}/RCR_{ADP/a,max} = 5$ μM ADP (Fig. 8C; Eq. 16). Similarly, 50% of the P/O_2 value is reached at an ADP control ratio of 2 (Fig. 8D). It may be argued that the traditional RCR should be inverted to obtain a quantity between 0 and 1 for a re-defined $RCR_{a/ADP}$. This yields a linearization of the ADP/O_2 flux ratio as a function of $RCR_{a/ADP}$ (see also Beavis and Lehninger (1986)), and 0.5 P/O_2 is reached at an inverted ADP control ratio of 0.5 (inset Fig. 8D; Eq. 17).

In summary, ADP limitation of respiration at high oxygen levels implies an over-proportionally steep decline of ADP flux (Fig. 9A), with the consequence of a hyperbolic decrease of the ADP/O_2 flux ratio as oxygen flux is reduced to the maintenance level at state 4 (Fig. 9B). Under hypoxia, in contrast, the ADP/O_2 flux ratio is maintained high even at extreme oxygen limitation of respiration in rat liver mitochondria (Fig. 9A and B). The same result was obtained with mitochondria isolated from the anoxia-tolerant brine shrimp embryos, *Artemia franciscana*, suggesting that this pattern represents a general bioenergetic response to low oxygen levels (Gnaiger et al., 2000b).

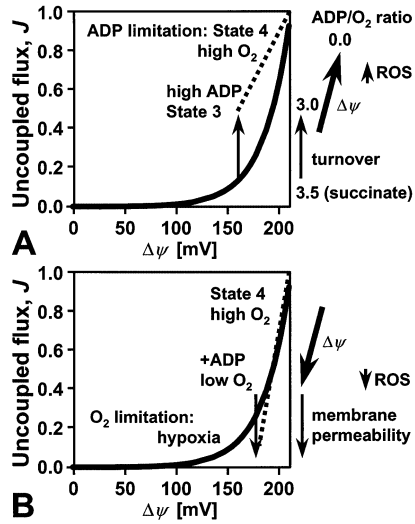

Fig. 10. Opposite effects of ADP limitation and oxygen limitation on mitochondrial membrane potential, Δψ, and uncoupled oxygen flux. (A) ADP limitation of respiration at high oxygen levels in the transition from the active state 3 to the resting state 4 leads to an increase of Δψ and exponential acceleration of the proton leak (heavy line). Because uncoupled oxygen flux increases while total oxygen flux is reduced, the ATP yield declines to zero. Turnover-dependent proton leaks increase the uncoupled oxygen flux at state 3, but decline towards state 4. Mitochondrial production of ROS increases with membrane potential towards state 4, and ROS-linked electron bypass contributes minimally to uncoupled oxygen flux at high oxygen. On the right, the decline of ADP/O_2 flux ratios is shown in the transition from state 3 to 4 (from Fig. 9B). (B) Oxygen limitation of respiration causes a reduction of Δψ in the transition from ADP limitation at high oxygen, to intracellular conditions of low oxygen and low ADP, to finally severe oxygen limitation under hypoxia and anoxia. Potentially synergistic with the well-documented Δψ effect on uncoupled flux, are the hypothetical effects of decreasing membrane permeability and suppression of ROS production under hypoxia.

4. The low-oxygen environment of the cell: mitochondria between hypoxic and oxidative stress

Comparison of mitochondrial respiratory control by oxygen and ADP suggests that several mechanisms are responsible for regulation of the ATP yield per unit oxygen consumed under physiological and hypoxic conditions. Some mechanisms are well understood, whereas others remain largely speculative at this time, as summarised in

Fig. 10. The decline of the ADP/O_2 flux ratio with reduction of respiration under the control of ADP (Fig. 9B) mainly reflects the decreasing proportion of proton flux into the mitochondrial matrix through the ATP synthase, relative to the proton leak. The mitochondrial membrane potential, $\Delta\psi$, and protonmotive force, Δp, increase with progressive ADP limitation in the transition from state 3 to 4, and the proton leak increases exponentially with $\Delta\psi$ (Garlid et al., 1989). The magnitude of uncoupled oxygen flux at various intensities of ADP-stimulated respiration, however, is a matter of debate. If the proton leak is a function of $\Delta\psi$ only (Beavis and Lehninger, 1986; Brand et al., 1993; Rolfe et al., 1999), then uncoupled respiration under state 3 conditions amounts to only 10–15% of state 4 (Hinkle et al., 1991). Thus, our results would correspond to a minimum estimate of 3.2 for the mechanistic P/O_2 ratio (Fig. 8). In addition to the $\Delta\psi$ effect, however, leak or slip increase as a function of electron flux and enzyme turnover rate (Fitton et al., 1994; Fontaine et al., 1997; Garlid et al., 1993). Then the mechanistic P/O_2 ratio is higher, and may be closer to or even underestimated by the linear slope of oxygen flux as a function of ADP flux (Fig. 9A). Mechanistically, the P/O_2 stoichiometry is calculated from proton ratios, H^+/O_2 of the proton pumps of the respiratory chain divided by H^+/ATP of the mitochondrial F_0F_1 ATP synthase. Including 1 H^+/ATP for the ATP/ADP antiporter, the H^+/ATP ratio is 4 (Hinkle et al., 1991). H^+/O_2 for cytochrome *c* oxidase is 8 (Verkhovsky et al., 1999). Estimates for site 2 vary between 4 and 8 (Beavis and Lehninger, 1986; Hinkle et al., 1991; Lemasters, 1984; Stoner, 1987). Taken together, these proton stoichiometries accommodate the range of directly measured ADP/O_2 flux ratios at state 3, up to the 'classical' stoichiometry of 4 P/O_2 for respiration with succinate. Ultimately, stoichiometries should be deduced from atomic structures of the molecular motors in motion (Stock et al., 1999), yet the actual performance of machines must be evaluated in studies of power output and efficiency. It is interesting to note that cytochrome *c* oxidase is competent to drive fully coupled proton translocation under conditions of oxygen limitation, when the enzyme starts the catalytic cycle form the fully reduced state (Verkhovsky et al., 1999).

Low oxygen levels in the intracellular environment under normoxic and hypoxic conditions exert profound effects on the relation between respiration and phosphorylation, with effects on uncoupled oxygen flux directly opposite to those of ADP limitation (Fig. 10). (a) Because the redox span of electron transport to oxygen is reduced under oxygen limitation (Gnaiger et al., 1995), the mitochondrial membrane potential declines in comparison to state 4 at experimentally elevated oxygen pressure (Fig. 10B). The loss of membrane potential is accentuated under anoxia and explains the depressed proton leak rate observed under these conditions, without a change of membrane permeability in the absence or presence of oxygen (St-Pierre et al., 2000a). This is consistent with the extreme condition of anoxia with minimum mitochondrial enzyme turnover, profound loss of membrane potential, and low proton leak even at air-level oxygen pressure, such that further anoxic membrane shutdown can hardly be detected. (b) Under conditions of nearly oxygen-saturated enzyme turnover at low intracellular oxygen levels, however, turnover-dependent uncoupled flux (Fig. 10A) may be compensated by a reduction of membrane permeability in an environment protected from a high-level oxidative stress (Fig. 10B; Gnaiger et al., 2000b). A strong dependence of cation permeability on respiratory enzyme turnover (Garlid et al., 1993; Fontaine et al., 1997) is not surprising in view of a 2/3 proportion of transmembrane proteins and only 1/3 phospholipids in the inner mitochondrial membrane (Skulachev, 1999).

Reduction of membrane permeability at low oxygen levels may be the specific result of a diminished production of ROS, or a purely thermodynamic and kinetic consequence of redox potentials in the respiratory chain and transmembrane electrochemical potentials. In support of the second alternative, one may compare effects on ADP/O_2 ratios induced by down-regulation on the output side of phosphorylation (low ADP concentration: comparable to low ATPase

activity, inhibition of translocase by carboxyatractyloside or of ATP synthesis by oligomycin) with limitations on the input side of the respiratory chain (low P_{O_2}; comparable to inhibition by malonate, antimycin A; for discussion see Gnaiger et al. (2000b)). It is well established, however, that oxidative stress induces damage to membranes, calcium cycling and opening of the mitochondrial permeability transition pore (Skulachev, 1999). (c) Compared to this indirect effect of ROS production on uncoupled flux, the direct effect of diverting electrons away from proton pumps as a result of superoxide production is small, since H_2O_2 production may account for $< 2\%$ of state 4 respiration (Boveris, 1977) or less in intact mitochondria in active or passive states (Staniek and Nohl, 2000). Reduction of ROS production under conditions of hypoxia (Costa et al., 1993), however, may contribute to maintain ADP/O_2 flux ratios high at low rates of oxygen-limited respiration.

Further studies are required before we may extend the findings of a depression of uncoupled respiration under severe hypoxia (Fig. 5B and C) to the intracellular condition of mild oxygen limitation of respiratory capacity under normoxia, when about 50% desaturation of myoglobin is observed (Conley et al., 2000; Molé et al., 1999). Importantly, competitive inhibition by NO will increase the P_{50} of mitochondrial respiration to oxygen and thus extend the range of oxygen limitation to much higher intracellular levels of P_{O_2} (Boveris et al., 1999; Brown, 2001; Cooper and Davies, 2000). Relative to the protective effects of a hypoxic microenvironment (Skulachev, 1996), the danger of an impairment of energy supply owing to hypoxia is more generally acknowledged. This paradigm of respiratory physiology may have to be extended, however, in view of the mitochondrial involvement in various oxygen-related pathologies such as ischemia-reperfusion injury, the mitochondrial theory of ageing, and apoptosis induced by mitochondrial defects. The advancement of a mitochondrial bioenergetics at intracellular and hypoxic oxygen levels, therefore, will contribute to a wide range of physiologically and clinically relevant topics.

Acknowledgements

Original research and instrumental development was supported by grants from FWF Austria (P7162-BIO) and FFF Austria (3/9357; 802985). I thank S.C. Hand, A.V. Kuznetsov, G. Méndez and B. Lassnig for co-operation and stimulating discussions.

References

Beavis, A.D., Lehninger, A.L., 1986. The upper and lower limits of the mechanistic stoichiometry of mitochondrial oxidative phosphorylation. Stoichiometry of oxidative phosphorylation. Eur. J. Biochem. 158, 315–322.

Boveris, A., 1977. Mitochondrial production of superoxide radical and hydrogen peroxide. In: Reivich, M., Coburn, R., Lahiri, S., Chance, B. (Eds.), Tissue Hypoxia and Ischemia. Thieme, Stuttgart, pp. 67–82.

Boveris, A., Costa, L.E., Cadenas, E., Poderoso, J.J., 1999. Regulation of mitochondrial respiration by ADP, O_2 and NO. Meth. Enzymol. 301, 188–198.

Brand, M.D., Harper, M.-E., Taylor, H.C., 1993. Control of the effective P/O ratio of oxidative phosphorylation in liver mitochondria and hepatocytes. Biochem. J. 291, 739–748.

Brown, G., 2001. Regulation of mitochondrial respiration by nitric oxide inhibition of cytochrome *c* oxidase. Biochim. Biophys. Acta 1504, 46–57.

Chance, B., Williams, G.R., 1955. Respiratory enzymes in oxidative phosphorylation. I. Kinetics of oxygen utilization. J. Biol. Chem. 217, 383–393.

Chance, B., Leigh, J.S., Clark, B.J., Maris, J., Kent, J., Nioka, S., Smith, D., 1985. Control of oxidative metabolism and oxygen delivery in human skeletal muscle: a steady-state analysis of the work/energy cost transfer function. Proc. Natl. Acad. Sci. 82, 8384–8388.

Cole, R.C., Sukanek, P.C., Wittenberg, J.B., Wittenberg, B.A., 1982. Mitochondrial function in the presence of myoglobin. J. Appl. Physiol. 53, 1116–1124.

Conley, K.E., Ordway, G.A., Richardson, R.S., 2000. Deciphering the mysteries of myoglobin in striated muscle. Acta Physiol. Scand. 168, 623–634.

Cooper, C.E., Davies, N.A., 2000. Effects of nitric oxide and peroxynitrite on the cytochrome oxidase K_m for oxygen: implications for mitochondrial pathology. Biochim. Biophys. Acta 1459, 390–396.

Costa, L.E., Llesy, S., Boveris, A., 1993. Active oxygen species in the liver of rats submitted to chronic hypobaric hypoxia. Am. J. Physiol. 264, C1395–C1400.

Costa, L.E., Méndez, G., Boveris, A., 1997. Oxygen dependence of mitochondrial function measured by high-resolution respirometry in long-term hypoxic rats. Am. J. Physiol. 273, C852–C858.

Fitton, V., Rigoulet, M., Ouhabi, R., Guérin, B., 1994. Mechanistic stoichiometry of yeast mitochondrial oxidative phosphorylation. Biochemistry 33, 9692–9698.

Fontaine, E.M., Devin, A., Rigoulet, M., Leverve, X., 1997. The yield of oxidative phosphorylation is controlled both by force and flux. Biochem. Biophys. Res. Comm. 232, 532–535.

Froncisz, W., Lai, C.S., Hyde, J.S., 1985. Spin-label oximetry kinetic study of cell respiration using a rapid-passage T_1-sensitive electron spin resonance display. Proc. Natl. Acad. Sci. USA 82, 411–415.

Garlid, K.D., Beavis, A.D., Ratkje, S.K., 1989. On the nature of ion leaks in energy-transducing membranes. Biochim. Biophys. Acta 976, 109–120.

Garlid, K.D., Semrad, C., Zinchenko, V., 1993. Does redox slip contribute significantly to mitochondrial respiration? In: Schuster, S., Rigoulet, M., Ouhabi, R., Mazat, J.-P. (Eds.), Modern Trends in Biothermokinetics. Plenum Press, New York, pp. 287–293.

Gayeski, T.E.J., Honig, C.R., 1991. Intracellular P_{O_2} in individual cardiac myocytes in dogs, cats, rabbits, ferrets, and rats. Am. J. Physiol. 260, H522–H531.

Gnaiger, E., Forstner, H. (Eds.), 1983. Polarographic Oxygen Sensors. Aquatic and Physiological Applications. Springer, Berlin, Heidelberg, New York, p. 370.

Gnaiger, E., 1993. Efficiency and power strategies under hypoxia. Is low efficiency at high glycolytic ATP production a paradox? In: Hochachka, P.W., Lutz, P.L., Sick, T., Rosenthal, M., Van den Thillart, G. (Eds.), Surviving Hypoxia: Mechanisms of Control and Adaptation. CRC Press, Boca Raton, Ann Arbor, London, Tokyo, pp. 77–109.

Gnaiger, E., Steinlechner-Maran, R., Méndez, G., Eberl, T., Margreiter, R., 1995. Control of mitochondrial and cellular respiration by oxygen. J. Bioenerg. Biomembr. 27, 583–596.

Gnaiger, E., Lassnig, B., Kuznetsov, A.V., Margreiter, R., 1998a. Mitochondrial respiration in the low oxygen environment of the cell. Effect of ADP on oxygen kinetics. Biochim. Biophys. Acta 1365, 249–254.

Gnaiger, E., Lassnig, B., Kuznetsov, A.V., Rieger, G., Margreiter, R., 1998b. Mitochondrial oxygen affinity, respiratory flux control, and excess capacity of cytochrome *c* oxidase. J. Exp. Biol. 201, 1129–1139.

Gnaiger, E., Kuznetsov, A.V., Schneeberger, S., Seiler, R., Brandacher, G., Steurer, W., Margreiter, R., 2000a. Mitochondria in the cold. In: Heldmaier, G., Klingenspor, M. (Eds.), Life in the Cold. Springer, Heidelberg, Berlin, New York, pp. 431–442.

Gnaiger, E., Méndez, G., Hand, S.C., 2000b. High phosphorylation efficiency and depression of uncoupled respiration in mitochondria under hypoxia. Proc. Natl. Acad. Sci. USA 97, 11080–11085.

Haller, T., Ortner, M., Gnaiger, E., 1994. A respirometer for investigating oxidative cell metabolism. Toward optimization of respiratory studies. Anal. Biochem. 218, 338–342.

Hochachka, P.W., Somero, G.N. (Eds.), 1984. Biochemical Adaptation. Princeton University Press, Princeton, p. 537.

Hinkle, P.C., Kumar, M.A., Resetar, A., Harris, D.L., 1991. Mechanistic stoichiometry of mitochondrial oxidative phosphorylation. Biochemistry 30, 3576–3582.

Jacobus, W.E., Moreadith, R.W., Vandegaer, K.M., 1982. Mitochondrial respiratory control. Evidence against the regulation of respiration by extramitochondrial phosphorylation potentials or by [ATP]/[ADP] ratios. J. Biol. Chem. 257, 2397–2402.

Jones, D.P., 1986. Intracellular diffusion gradients of O_2 and ATP. Am. J. Physiol. 250, C663–C675.

Kramer, R.S., Pearlstein, R.D., 1983. Reversible uncoupling of oxidative phosphorylation at low oxygen tension. Proc. Natl. Acad. Sci. USA 80, 5807–5811.

Kreutzer, U., Jue, T., 1995. Critical intracellular O_2 in myocardium as determined by ^1H nuclear magnetic resonance signal of myoglobin. Am. J. Physiol. 268, H1675–H1681.

Lassnig, B., Kuznetsov, A.V., Margreiter, R., Gnaiger, E., 1998. Aerobic-anoxic transitions and regulation of mitochondrial oxygen flux. In: Larsson, C., Påhlman, I.-L., Gustafsson, L. (Eds.), BioThermoKinetics in the Post Genomic Era. Chalmers Reproservice, Göteborg, pp. 312–316.

Lemasters, J.J., 1984. The ATP-to-oxygen stoichiometries of oxidative phosphorylation by rat liver mitochondria. An analysis of ADP-induced oxygen jumps by linear nonequilibrium thermodynamics. J. Biol. Chem. 259, 13123–13130.

Méndez, G., Gnaiger, E., 1994. How does oxygen pressure control oxygen flux in isolated mitochondria? A methodological approach by high-resolution respirometry and digital data analysis. In: Gnaiger, E., Gellerich, F.N., Wyss, M. (Eds.), What is Controlling Life? Modern Trends in BioThermoKinetics 3. Innsbruck University Press, Innsbruck, pp. 191–194.

Molé, P.A., Chung, Y., Tran, T.K., Sailasuta, N., Hurd, R., Jue, T., 1999. Intracellular P_{O_2} and bioenergetic measurements in skeletal muscle: the role of exercise paradigm. Am. J. Physiol. 277, R173–R180.

Reck, M., Wyss, M., Lassnig, B., Gnaiger, E., 1997. High time resolution. OROBOROS Bioenerg. News 2.4, 1–13.

Rolfe, D.F.S., Newman, J.M.B., Buckingham, J.A., Clark, M.G., Brand, M.D., 1999. Contribution of mitochondrial proton leak to respiration rate in working skeletal muscle and liver and to SMR. Am. J. Physiol. 276, C692–C699.

Rumsey, W.L., Schlosser, C., Nuutinen, E.M., Robiolio, M., Wilson, D.F., 1990. Cellular energetics and the oxygen dependence of respiration in cardiac myocytes isolated from adult rat. J. Biol. Chem. 265, 15392–15402.

Sharpe, M.A., Cooper, C.E., 1998. Interaction of peroxynitrite with mitochondrial cytochrome oxidase: catalytic production of nitric oxide and irreversible inhibition of enzyme activity. J. Biol. Chem. 273, 30961–30972.

Skulachev, V.P., 1996. Role of uncoupled and non-coupled oxidations in maintenance of safely low levels of oxygen and its one-electron reductants. Quart. Rev. Biophys. 29, 169–202.

Skulachev, V.P., 1999. Mitochondrial physiology and pathology; concepts of programmed cell death of organelles, cells and organisms. Mol. Asp. Med. 20, 139–184.

Staniek, K., Nohl, H., 2000. Are mitochondria a permanent source of reactive oxygen species? Biochim. Biophys. Acta 1460, 268–275.

Steinlechner-Maran, R., Eberl, T., Kunc, M., Margreiter, R., Gnaiger, E., 1996. Oxygen dependence of respiration in coupled and uncoupled endothelial cells. Am. J. Physiol. 271, C2053–C2061.

Stock, D., Leslie, A.G.W., Walker, J.E., 1999. Molecular architecture of the rotary motor in ATP synthase. Science 286, 1700–1705.

Stoner, C.D., 1987. Determination of the P/2e$^-$ stoichiometries at the individual coupling sites in mitochondrial oxidative phosphorylation. Evidence for maximum values of 1.0, 0.5, and 1.0 at sites 1, 2 and 3. J. Biol. Chem. 262, 11445–11453.

St-Pierre, J., Brand, M.D., Boutilier, R.G., 2000a. Mitochondria as ATP consumers: cellular treason in anoxia. Proc. Natl. Acad. Sci. USA 97, 8670–8674.

St-Pierre, J., Tattersall, G.J., Boutilier, R.G., 2000b. Metabolic depression and enhanced O_2 affinity of mitochondria in hypoxic hypometabolism. Am. J. Physiol. 279, R1205–R1214.

Takahashi, E., Endoh, H., Doi, K., 1999. Intracellular gradients of O_2 supply to mitochondria in actively respiring single cardiomyocyte of rats. Am. J. Physiol. 276, H718–H724.

Verkhovsky, M.I., Morgan, J.E., Puustinen, A., Wikström, M., 1996. Kinetic trapping of oxygen in cell respiration. Nature 380, 268–270.

Verkhovsky, M.I., Jasaitis, A., Verkhovskaya, M.L., Morgan, J.E., Wikström, M., 1999. Proton translocation by cytochrome *c* oxidase. Nature 400, 480–483.

Wilson, D.F., Owen, C.S., Erecinska, M., 1979. Quantitative dependence of mitochondrial oxidative phosphorylation on oxygen concentration: a mathematical model. Arch. Biochem. Biophys. 195, 494–504.

Wittenberg, B.A., Wittenberg, J.B., 1985. Oxygen pressure gradients in isolated cardiac myocytes. J. Biol. Chem. 260, 6548–6554.

Wittenberg, B.A., Wittenberg, J.B., 1989. Transport of oxygen in muscle. Ann. Rev. Physiol. 51, 857–878.